American Mineralogist, Volume 79, pages 107–112, 1994

Structural relaxation of the chlorite surface imaged by the atomic force microscope

Gordon A. Vrdoljak, Grant S. Henderson, J. Jeffrey Fawcett
Department of Geology, 22 Russell Street, University of Toronto, Toronto, Ontario M5S 3B1, Canada
Frederick J. Wicks
Department of Mineralogy, Royal Ontario Museum, 100 Queen's Park, Toronto, Ontario M5S 2C6, Canada

Abstract

The surface structure of the layer silicate mineral chlorite has been imaged at near-atomic resolution using an atomic force microscope (AFM). The chlorite structure consists of a 2:1 talc-like layer and a brucite-like interlayer sheet. The AFM clearly resolves the OH groups of the brucite-like interlayer sheet and the bases of the SiO_4 tetrahedra of the talc-like sheet. The imaged surface structures of both the talc- and brucite-like layers are generally consistent with that of the bulk structure. The mean unit-cell distances (a = 5.31 ± 0.31, b = 9.74 ± 0.80 Å) are within 1 and 5%, respectively, of those calculated for the known structure. However, some structural relaxation of the talc-like surface is observed. This relaxation manifests itself as a systematic shortening and elongation of both a and b across the layer and probably results from a concertina-like readjustment of the surface after cleaving. The brucite-like layer does not exhibit similar behavior.

Introduction

Many geochemical phenomena such as mineral dissolution, precipitation and growth, cation adsorption and desorption, and trace-element cycling are highly dependent upon the physical and chemical behavior of mineral surfaces (Hochella and White, 1990). The structure and topology of the surface itself are particularly important, as they directly affect reaction rates and mechanisms.

The development of the atomic force microscope (AFM) has enabled the structure of insulator surfaces such as silicate minerals to be readily imaged at very high resolution. Images of the surfaces of calcite (Rachlin et al., 1992), zeolite (Weisenhorn et al., 1990), albite (Drake and Hellmann, 1991), illite-smectite (Lindgreen et al., 1991), and lizardite (Wicks et al., 1992) have been obtained at near-atomic or molecular resolution. Phyllosilicate minerals, composed of flat sheets of three corner-sharing SiO_4 tetrahedra, are particularly suitable for study by AFM because of their perfect cleavage along the {001} plane. Imaging of the {001} surface of the 2:1 sheet silicate muscovite shows molecular resolution of the individual tetrahedra for the tetrahedral sheet (Drake et al., 1989).

Lizardite is a 1:1 phyllosilicate consisting of a single tetrahedral and octahedral sheet as its basic repeat unit. Atomic resolution of the OH groups and the Mg atoms has been obtained in the octahedral sheet, and molecular resolution of the SiO_4 tetrahedra has been obtained in the tetrahedral sheet (Wicks et al., 1992). The 1:1 sheet silicates and the 2:1 sheet silicates with an interlayer hydroxide sheet exhibit three structurally different {001} surfaces (octahedral, tetrahedral, and interlayer hydroxide sheets), and it should be possible to image both the tetrahedral and octahedral or interlayer hydroxide surfaces within the same sample.

Chlorite group minerals are 2:1 phyllosilicates with an interlayer brucite-like sheet that incorporates medium-sized cations such as Mg, Al, and Fe in the octahedral sites. The 2:1 talc-like layer consists of two tetrahedral sheets of SiO_4 tetrahedra, with an octahedral sheet sandwiched between the two tetrahedral sheets. In chlorite this talc-like layer has a general composition of $(R^{2+}, R^{3+})_3(Si_{4-x}Al_x)O_{10}(OH)_2$, where R = Mg, Fe, or Al. The excess negative charge is neutralized by the positively charged octahedral brucite-like interlayer sheet of composition $(R^{2+}, R^{3+})_3(OH)_6$ (R = Mg, Fe). The chlorite structure is presented in Figure 1 (Bailey, 1988). In this study we have investigated a clinochlore IIb chlorite sample with composition $(Mg_{4.4}Fe_{0.6}Al)(Si_{2.9}Al_{1.1})O_{10}(OH)_8$, obtained from northern Ontario.

Experimental details

Samples were cleaved along {001} using a scalpel, and both halves were examined in air using a Digital Instruments Nanoscope III AFM with a vibration isolation platform. Contact forces were on the order of ≤20–150 nN and were adjusted to optimize image resolution. A wide range of scan rates and scan directions were used. The AFM scanner was calibrated against mica and Au ruling standards, and thermal drift was minimized by allowing the AFM to equilibrate with the surrounding air temperature. Images identified as having excessive drift were discarded.

It was found that Au-coated Si_3N_4 cantilevers with legs

0003–004X/94/0102–0107$02.00

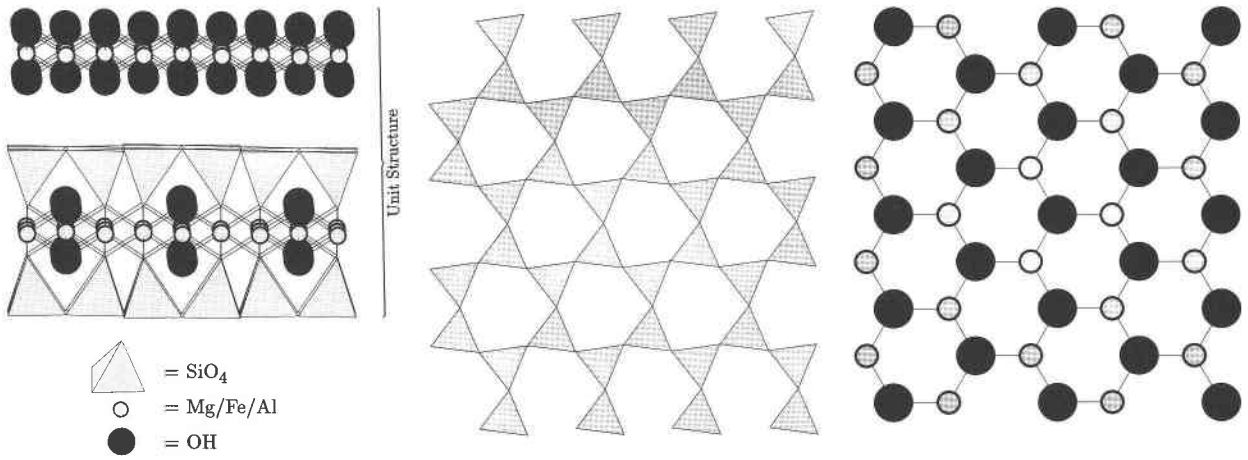

Fig. 1. **(Left)** Schematic of the unit structure of chlorite showing the 2:1 talc-like layer and brucite-like interlayer sheet; **(middle)** {001} projection of the siloxane sheet of the talc-like layer; **(right)** {001} projection of the upper surface of the brucite-like interlayer sheet.

200 μm wide were best for imaging the tetrahedral sheet, whereas the 100-μm-leg versions were more effective for the brucite-like interlayer sheet. All structural features discussed in the text were visible in the raw (= unfiltered) images, but standard digital filtering techniques were performed to improve the quality of the images, and every effort was made not to introduce artifacts into the processed image. This was checked by careful monitoring of interatomic distances and atom positions before and after application of the filtering routines. Observed images were compared with talc- and brucite-like structures calculated from a IIb chlorite (corrected for our composition) of Bailey, (1975).

To facilitate comparison between the talc- and brucite-like layers, all images have been filtered in the same manner. The filtering options used are flatten, low-pass, and two-D fast Fourier filtering (FFT). In some figures the intensity distribution across the image appears to vary. This variation is related to the color contrast and offset and the FFT parameters employed during the filtering. Different filtering and color contrast and offset parameters change the intensity distributions but do not alter the instrumentally induced ditrigonal symmetry nor the postulated Mg atom positions (see below).

The flatten routine subtracts the average value of height along each scan line from each point in the line and is applied to remove any image bow. Low-pass filtering replaces each pixel with a weighted average of the 3 × 3 cell of pixels surrounding and including the original pixel and removes spot noise; the two-D FFT calculates periodicities observed in the image (it is somewhat comparable to a LEED image of the surface). These periodicities may then be selected (or rejected) for incorporation into the inverse transform, which produces an image significantly reduced in noise. However, one must be careful that information is not lost, and in general the two-D FFT is used to highlight features that are already observable in the unfiltered images.

Results and discussion

Raw and filtered images of the talc-like layer are shown in Figure 2. The {001} surface of the 2:1 talc-like layer is seen to consist of an array of hexagonal rings of SiO_4 tetrahedra (Fig. 2C), consistent with the known crystal structure. There is very good agreement between the observed and calculated structure of the silicate sheet of the talc-like layer, and the mean observed unit-cell distances ($a = 5.31 \pm 0.31$, $b = 9.74 \pm 0.80$ Å) agree within 1 and 5%, respectively, of the calculated values. This close correspondence between the structure observed in the images and the cell structure calculated from known atom positions determined by X-ray structure analysis is strong evidence that we are obtaining true atomic or near-atomic resolution (cf. Ohnesorge and Binnig, 1993).

Rotation of the tetrahedra within the {001} plane of the siloxane sheet (see Fig. 1 middle) reduces the hexagonal symmetry of the SiO_4 rings to ditrigonal (Brown and Bailey, 1963). This ditrigonal symmetry is observed in Figure 2D as distortions of the hexagonal SiO_4 rings, with each ring appearing to point in a defined direction (see Fig. 2D). The magnitude of the in-plane rotation could not be determined, as the images do not resolve the bridging O atom between adjacent SiO_4 tetrahedra.

However, the tetrahedra around each hexagonal ring also exhibit an apparent rotation of up to 18° (mean = 6.96 ± 4.38°) out of the **a-b** plane. This is seen in the images as alternating highs and lows in image intensity for each tetrahedra within individual six-membered SiO_4 rings. This apparent rotation further emphasizes the real ditrigonal symmetry but is purely an instrumental artifact. It is observed in other sheet structures, such as graphite, mica, and 1:1 layer silicates (Gould et al., 1989), and theoretical calculations of tip-sample interactions indicate that it probably results from an asymmetric (two atom) cantilever tip (Gould et al., 1989).

In an attempt to quantify surface relaxation effects and

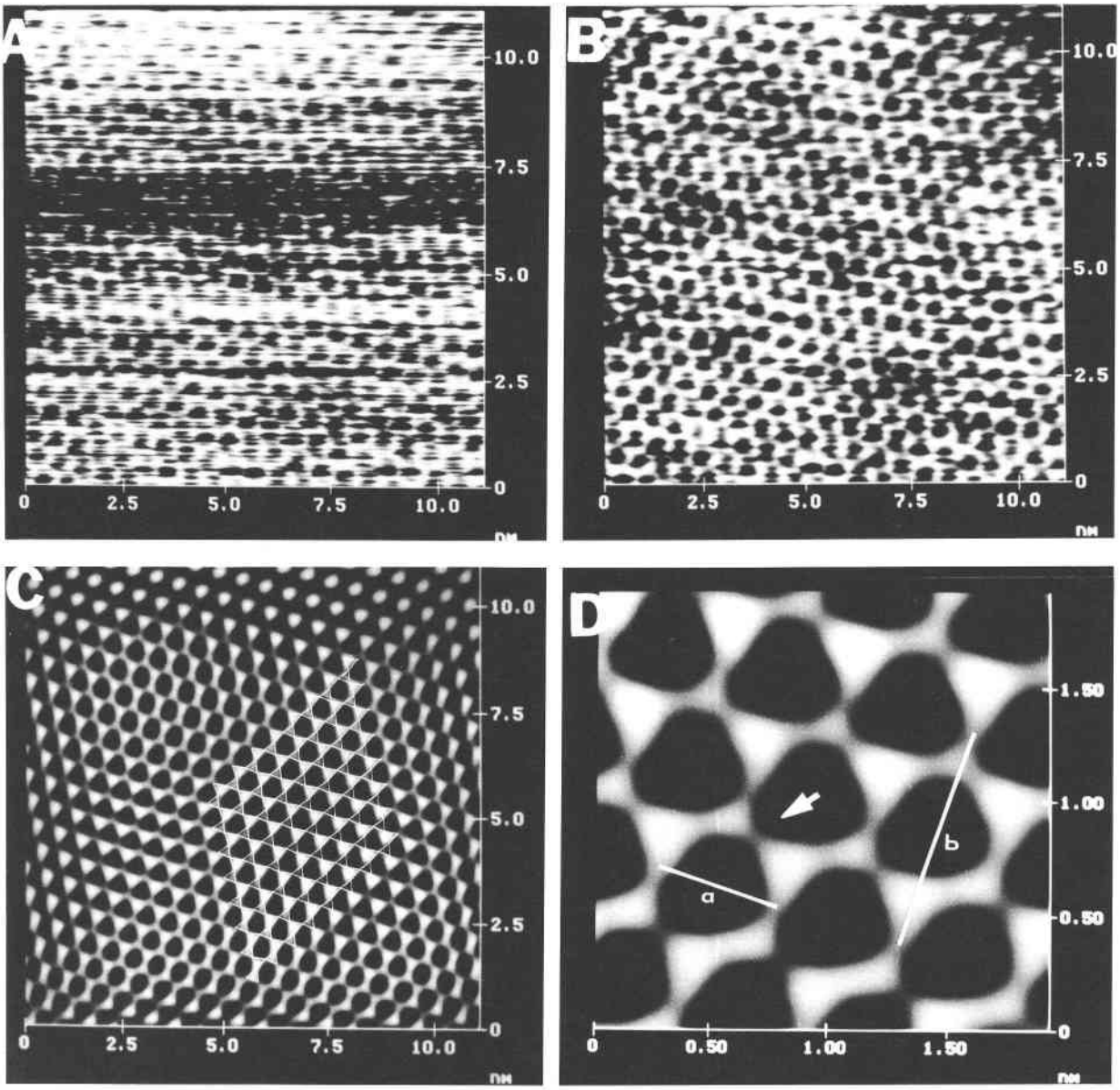

Fig. 2. Images of the siloxane sheet of the talc-like layer: (**A**) typical raw image; (**B**) image after application of flattening and low-pass filtering routines; (**C**) image shown in **B** after application of two-D FFT to increase the resolution further. The overlay is the talc-like layer (cf. Fig. 1 **middle**), calculated from the chlorite structure of Bailey (1975) (see text). Note that the theoretical and experimental structures essentially match. (**D**) Enlarged view of **C** clearly showing the tip-induced rotations out of the **a-b** plane (seen as alternating bright and dark tetrahedra within the rings). Unit-cell dimensions are indicated. The arrow indicates the direction a six-membered SiO_4 ring is pointing because of the tetrahedral rotations described by Brown and Bailey (1963).

to determine if there is a systematic spatial relationship to any relaxation, ~700 measurements of a and b distances were performed on a single image of the talc-like layer. (The image used is Fig. 2C.) It was found that the b unit-cell distances tend to vary (variance = 0.632) more than those of a (variance = 0.1). In addition, both a and b dimensions essentially cluster around specific values (see Fig. 3). Greater than 99% of the a and b measurements fall around the following values: a = 5.47, 5.86, 6.26 and b = 8.98, 9.37, 9.77, 10.16 Å. These values indicate that the cell dimensions undergo a systematic change of ~±0.4 Å with both a and b varying equally. This is expected if the ditrigonal symmetry of the surface is maintained; if the surface symmetry were not ditrigonal, then the variation in a and b would be nonequivalent.

The variation in cell dimensions could result from thermal drift of the instrument, tip-induced deformation

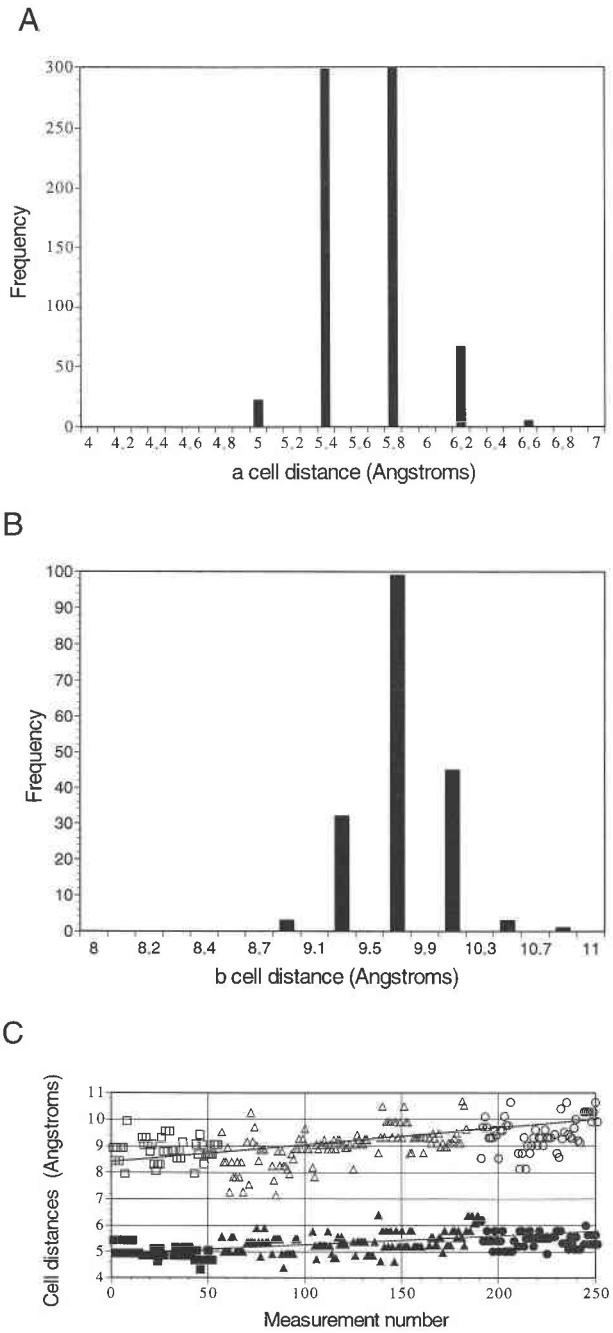

Fig. 3. (**A**) Histogram of measured *a* cell distances (ångströms). (**B**) Histogram of measured *b* cell distances (ångströms). All measurements are from a single image (Fig. 2) of the talc-like layer; >90% of the measurements fall within four values. (**C**) Two hundred fifty measured cell distances (ångströms) taken from some 15–20 images of the talc-like layer in air (square), oil (triangle), and H_2O (circle). Solid symbols are *a* cell distances and open symbols are *b* cell distances. Linear regression analysis indicates expansion of the *b* dimension ($r = 0.4587$) and to a lesser extent *a* ($r = 0.4544$) upon the addition of H_2O to the surface.

of the surface, an artifact, the algebraic correction for nonlinearity of the piezo or of calibration of the instrument to a standard with similar dimensions (in this case muscovite), or relaxation of the surface. Thermal drift of the instrument and tip-induced surface deformation seem unlikely, since only slight differences are observed for *a* and *b* measurements, even when scan speed and direction, contact force, cantilever type, sample, and imaging medium are varied. Images of the same talc-like layer in air, oil, and H_2O exhibit essentially the same behavior in *a* and *b*.

Figure 3C is a plot of measured unit-cell distances taken from a number of images of the talc-like layer in air, oil, and H_2O. It is clear that although the variation in both *a* and *b* is somewhat greater for these measurements relative to those from the single image, the *a* and *b* dimensions do exhibit similar behavior to that of the single image in air. Further, linear regression of the data indicates that both cell dimensions appear to increase slightly on going from air to H_2O. This slight increase of *a* and *b* in H_2O presumably occurs as the talc-like layer is rehydrated in solution, with H_2O molecules entering the siloxane ring and expanding the structure.

We believe that the observed variation in *a* and *b* is probably due to relaxation of the surface. However, we cannot rule out the possibility of an instrumental artifact produced by the piezo nonlinearity correction or instrument calibration. Any instrumental artifact should also generate similar behavior in images of the brucite-like layer, but no such variation in the *a* cell dimension is observed (see below). If the variation in cell parameters is real, then the surface relaxation is presumably a consequence of surface decompression after cleaving and readjustment of the negatively charged talc-like layer to compensate for the lack of an overlying charge-balancing brucite-like interlayer sheet. The mechanism by which that occurs may be a concertina-like compression of the surface, producing both shortening and elongation of cell dimensions.

The brucite-like interlayer sheet (Fig. 4) has trigonal symmetry, as expected. The OH sheet is readily seen (Fig. 4C, 4D), and the measured mean *a* unit-cell distance (shown in Fig. 4D) is within 2% (5.40 ± 0.18 Å) of the calculated *a* value of 5.31 Å. No corresponding rotation out of the **a-b** plane was observed at low contact forces, but rotation was observed when higher contact forces were used. The measured *a* distances, although variable, are random and do not exhibit a systematic variation similar to that observed for the talc-like layer. Comparison of the imaged structure with a calculated brucite-like interlayer sheet shows a very close correspondence between the OH atoms of the calculated structure (large spheres) and the OH positions in the image (Fig. 4C).

There is also a good correspondence between the calculated Mg positions (small circles in Fig. 4C) and regions of the image where we believe the Mg cations of the $Mg(OH)_6$ groups can be seen in the center of a triangle of

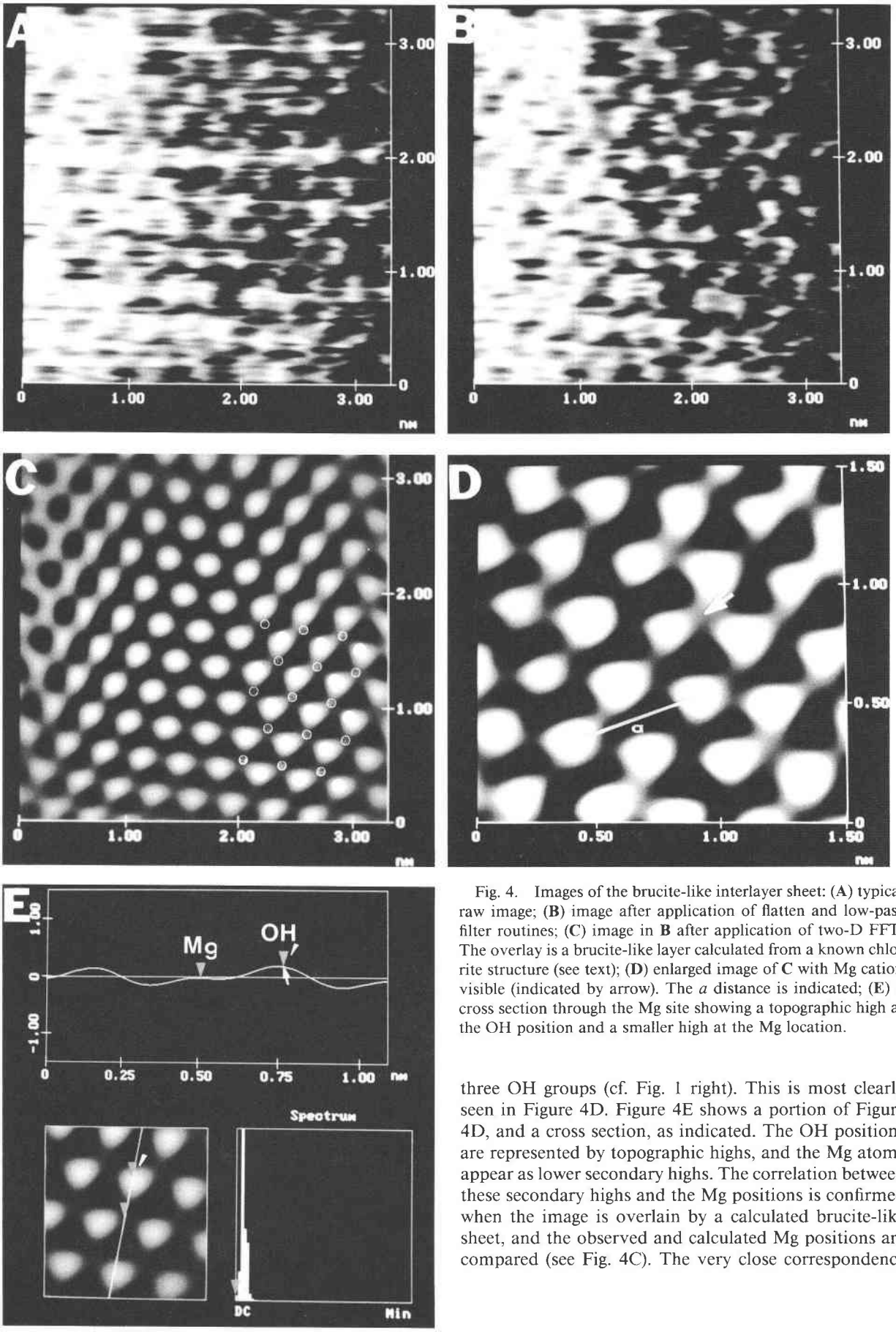

Fig. 4. Images of the brucite-like interlayer sheet: (**A**) typical raw image; (**B**) image after application of flatten and low-pass filter routines; (**C**) image in **B** after application of two-D FFT. The overlay is a brucite-like layer calculated from a known chlorite structure (see text); (**D**) enlarged image of **C** with Mg cation visible (indicated by arrow). The *a* distance is indicated; (**E**) a cross section through the Mg site showing a topographic high at the OH position and a smaller high at the Mg location.

three OH groups (cf. Fig. 1 right). This is most clearly seen in Figure 4D. Figure 4E shows a portion of Figure 4D, and a cross section, as indicated. The OH positions are represented by topographic highs, and the Mg atoms appear as lower secondary highs. The correlation between these secondary highs and the Mg positions is confirmed when the image is overlain by a calculated brucite-like sheet, and the observed and calculated Mg positions are compared (see Fig. 4C). The very close correspondence

between the calculated brucite-like structure and the regions that we believe to be Mg atoms makes it very unlikely that the features in the image are due to anything other than Mg. It would be truly fortuitous if these features were instrumental artifacts that always happened to occur at positions in the image where one would expect the Mg atoms to occur.

Much of the bonding between layers within phyllosilicate minerals is due to weak Van der Waals forces and H bonding. Scanning the surface of these materials with high contact forces strips away weaker bonded surface layers. Thus it is possible to image progressively the upper tetrahedral, the octahedral, and the bottom tetrahedral sheets of the 2:1 talc-like layer. Images obtained in this manner generally agreed with the expected bulk structure but tended to be damaged by the cantilever. However, the possibility exists that the AFM may be used to construct a depth profile of the structure of minerals and to determine the polytype directly.

It is clear that it is possible to obtain near-atomic resolution images of both the talc-and brucite-like layers in 2:1 phyllosilicates using the AFM. Careful analysis of the images also shows that, although the surface structure closely resembles that of the known mineral, there is significant relaxation at the surface. The AFM may be used to image other structural features on the near-atomic scale, such as domain structures, and to image progressively descending layers in the structure.

Acknowledgments

This work was funded by Natural Science and Engineering Research Council of Canada operating and equipment grants to G.S.H. Reviews by two anonymous referees and S.W. Bailey greatly improved the manuscript.

References cited

Bailey, S.W. (1975) Chlorites. In J.E. Gieseking, Ed., Soil components, p. 191–263. Springer-Verlag, New York.

——— (1988) Chlorites: Structures and crystal chemistry. In Mineralogical Society of America Reviews in Mineralogy, 19, 347–403.

Brown, B.E., and Bailey, S.W. (1963) Chlorite polytypism. II. Crystal structure of a one-layer Cr-chlorite. American Mineralogist, 48, 42–61.

Drake, B., and Hellmann, R. (1991) Atomic force microscopy imaging of the albite (010) surface. American Mineralogist, 76, 1773–1776.

Drake, B., Prater, C.B., Weisenhorn, A.L., Gould, S.A.C., Albrecht, T.R., Quate, C.F., Connell, D.S., Hansma, H.G., and Hansma, P.K. (1989) Imaging crystals, polymers, and processes in water with the atomic force microscope. Science, 243, 1586–1589.

Gould, S.A.C., Burke, K., and Hansma, P.K. (1989) Simple theory for the atomic-force microscope with a comparison of theoretical and experimental images of graphite. Physical Review, 40, 5363–5366.

Hochella, M.F., Jr., and White, A.F. (1990) Mineral-water interface geochemistry: An overview. In Mineralogical Society of America Reviews in Mineralogy, 23, 1–16.

Lindgreen, H., Gaenees, J., Hansen, P.L., Besenbacker, F., Laesgaard, E., Stensgaard, I., Gould, S.A.C., and Hansma, P.K. (1991) Ultrafine particles of North Sea illite/smectite clay minerals investigated by STM and AFM. American Mineralogist, 76, 1218–1222.

Ohnesorge, F., and Binnig, G. (1993) True atomic resolution by atomic force microscopy through repulsive and attractive forces. Science, 260, 1451–1456.

Rachlin, A.L., Henderson, G.S., and Goh, C. (1992) An atomic force microscope (AFM) study of the calcite cleavage plane: Image averaging in Fourier space. American Mineralogist, 77, 904–910.

Weisenhorn, A.L., MacDougall, J.E., Gould, S.A.C., Cox, S.D., Wise, W.S., Massie, J., Maivald, P., Elings, V.B., Stucki, G.D., and Hansma, P.K. (1990) Imaging and manipulating molecules on a zeolite surface with an atomic force microscope. Science, 247, 1330–1333.

Wicks, F.J., Kjoller, K., and Henderson, G.S. (1992) Imaging of the hydroxyl surface of lizardite at atomic resolution with the atomic force microscope. Canadian Mineralogist, 30, 83–91.

Manuscript received March 3, 1993
Manuscript accepted September 15, 1993